Mobi^{2}Sense: Empowering Wireless Sensing with Mobility

Fusang Zhang[†*], Jie Xiong[‡], Zhaoxin Chang[§†], Junqi Ma[†*], Daqing Zhang[§♯]
[†] Institute of Software, Chinese Academy of Sciences, [*] University of Chinese Academy of Sciences,
[‡] University of Massachusetts Amherst, [§] Telecom SudParis, Institut Polytechnique de Paris, [♯] Peking University
fusang@iscas.ac.cn, jxiong@cs.umass.edu, zhaoxin.chang@telecom-sudparis.eu,
majunqi22@otcaix.iscas.ac.cn, daqing.zhang@telecom-sudparis.eu

ABSTRACT

Besides the conventional communication function, wireless signals are actively exploited for sensing purposes recently. However, a missing component of existing wireless sensing is sensing under device motions. This is challenging because device motions can easily overwhelm target motions such as chest displacement used for respiration sensing. This paper takes a first step in the direction of involving device mobility into the ecosystem of wireless sensing. Owning to the miniaturization and low cost of ultra-wideband (UWB) chip in recent years, we propose to integrate the accuracy of UWB sensing with mobility to support truly ubiquitous wireless sensing. We propose Mobi^{2}Sense, a system design to support sensing under device motions. We propose novel signal processing schemes to remove the effect of device motions on sensing and prototype Mobi^{2}Sense using commodity UWB hardware. Real-world applications demonstrate that even in the presence of device motions, fine-grained Mobi^{2}Sense is able to capture subtle target motions to "hear" music, "see" human respiration, and "recognize" multi-target gestures at a high accuracy.

CCS CONCEPTS

• **Human-centered computing** → **Ubiquitous and mobile computing systems and tools**.

KEYWORDS

wireless sensing, RF sensing, ultra-wideband (UWB) sensing, integration of wireless sensing and mobility, device motion removal, interference mitigation

1 INTRODUCTION

Recent years have witnessed the rapid progress of sensing using various wireless signals including WiFi [3, 60, 62], RFID [22, 56], mmWave [29, 52], ultrasound [36, 44, 67] and LoRa [18, 63, 64]. The contact-free and sensor-free nature of wireless sensing is appealing in many real-life scenarios. A large range of applications have been enabled by wireless sensing including activity tracking [26, 32, 66], gesture recognition [3, 28, 53], respiration monitoring [45, 59, 73] and vibration sensing [6, 66]. While promising progress has been achieved, one interesting observation about existing wireless sensing systems is that the transmitter and receiver are always static (e.g., placed on a desk or mounted on the ceiling). However, it is noted that in some real-life scenarios, the wireless device can be non-static. For example, as shown in Figure 1, a smartphone can be held in hand by a user to sense a target. A moving robot equipped with wireless sensing modules moves around to sense the surroundings. Therefore, an important missing piece of wireless sensing is sensing under device motions.

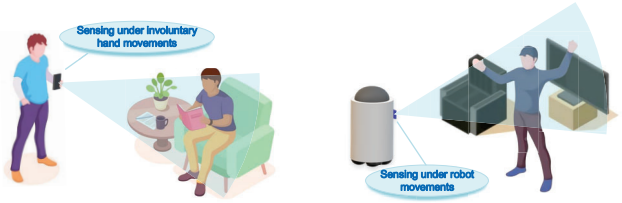

Figure 1: Wireless sensing in the presence of device motions.

In this paper, we consider device mobility in wireless sensing for the first time. To see the effect of device motions on sensing, we conduct a range of benchmark experiments. Surprisingly, we find that wireless sensing stops working when the wireless device is placed on a moving robot. Even under subtle involuntary hand movement when the device (e.g., a smartphone) is held in hand, the sensing performance is severely degraded as shown in Figure 2.

After a thorough analysis, we realize that this is because the fundamental principle of wireless sensing is that target movement causes signal variation and therefore the target context (e.g., movement speed and direction) can be obtained by analyzing the signal variation. However, this fundamental principle does not hold when a wireless device starts moving. Under device motions, the signal reflected from target contains movement information of both target and device. For fine-grained human respiration monitoring, even subtle involuntary hand movement can fail sensing.

Another observation is that when wireless signals are used for sensing, the original communication function is usually compromised. Take WiFi as the example, the packet size and packet interval need to be precisely controlled to enable sensing [2, 48]. WiFi sensing is therefore not feasible in real WiFi environment with random back-offs and varying packet sizes. This is a big issue hindering WiFi sensing being adopted in real life. The small frequency bandwidth of WiFi also limits the granularity of WiFi sensing. In contrast, UWB is used for ranging and extending its usage for sensing does not compromise the original function of UWB.

In this paper, we employ commodity UWB hardware for sensing. We believe UWB is a promising candidate to push wireless sensing for real-world adoption with several unique advantages: (i) finer sensing granularity because of a much larger frequency bandwidth;

ACM MobiCom '22, October 17–21, 2022, Sydney, NSW, Australia

ACM ISBN 978-1-4503-9181-8/22/10.
https://doi.org/10.1145/3495243.3560518

Figure 2: Signal of respiration under device motions.

(ii) does not compromise its original function; (iii) lower power consumption which is critical for battery-powered mobile devices (e.g., a smartphone) owing to the pulse signal design.

With so many advantages, the reason why UWB sensing was not popular is mainly due to the large size and high hardware cost. Recent advancements in semiconductor technologies dramatically miniaturize the hardware size and reduce the cost. UWB chip can now be integrated into consumer electronics, much like accelerometers and CMOS cameras. From 2019, UWB chip is a default component in iPhone [10]. Samsung and Xiaomi follow this trend to include UWB chip in their latest smartphones [8, 41]. Lenovo also recently integrates UWB chip in their laptops [25]. For robot, UWB has long been utilized for positioning [20]. We envision UWB to be even more popular and available in lots of consumer electronics in the near future.

In this paper, we involve device mobility into the ecosystem of wireless sensing and employ UWB hardware as our sensing platform. We ask this question: *while device motion breaks the fundamental principle of wireless sensing, how to model the effect of device motion on sensing and address it to enable wireless sensing?*

In wireless sensing, the propagation signals are grouped as static signal and dynamic signal. Signals reflected from walls and furniture are static signals while signals reflected from a moving target are dynamic signals. The target information is contained in the dynamic signal. However, under device motions, there is no static signal any more. The signals reflected from a static object (e.g., a wall) are also dynamic due to device motions. Existing sensing models can not be applied and traditional methods used to remove static signals such as background subtraction [19] do not work any more. In this paper, we seek to derive the theoretical model to quantify the effect of device motions on sensing.

However, removing the effect of device motions is a non-trivial task. When a device is held in hand, the motion pattern can be quite random. For robot movements, although the moving speed and direction can be obtained from IMU sensors, it is very difficult to capture the finer-grained device vibrations and jitters which still affect the sensing of subtle target motions such as respiration. Existing sensors on robots, including cameras and Lidar, have a strong capability to image targets. However, the micro-movement of targets (e.g., human respiration) is difficult to be captured using these sensors. Also, these sensors can be blocked by occlusions and can not work in low-visibility scenarios (e.g., smoke and fog). We envision wireless sensing can be integrated with existing sensing modalities to achieve even more powerful sensing capabilities.

In this work, we propose a novel method which is capable of removing random device motions to enable fine-grained sensing. The basic idea is to employ one static object in the environment as a reference to cancel out the effect of device movement. The reference can be commonly-seen static objects such as a wall, a desk, a laptop or even a water bottle. The reflection from static object contains only the device motion. In contrast, the reflection from the target contains both device motion and target motion. Removing the device motion is non-trivial and we face two challenges: i) Device motion is not a signal but just causes the signal to vary. Traditional methods such as interference cancellation [37, 43] can not be applied here; ii) The device motion viewed at the target and the device motion viewed at the reference static object are different. Therefore, the device motion can not be easily cancelled out.

In this paper, we model the effect of device motion on signal variation. We cancel the signal variation caused by device motion through a division operation between signal reflected from the target and signal reflected from the static reference. To tackle the inconsistency of viewing device motions at different locations, we convert the signal variation caused by device motion at the reference to that at the target to make them consistent for cancellation. We demonstrate the correctness of the proposed method both theoretically and experimentally.

We implement the proposed sensing system Mobi^{2}Sense using commodity UWB hardware and conduct comprehensive experiments in two typical mobility scenarios, i.e., hand-held mobility scenario and robot-carried mobility scenario. We further showcase three applications of different target motion scales: i) employing the proposed system to sense sub-millimeter level vibration of a speaker to "hear" the music in the presence of device motions; ii) holding the UWB device in hand to accurately monitor the patient's millimeter level respiration (rate and depth) in a real hospital environment; and iii) placing the UWB device on a moving robot to simultaneously recognize gestures of multiple targets. For all three applications, our system achieves highly accurate sensing performance. The demo video can be found at https://youtu.be/ATOmMkGwIUw. The main contributions of our work are summarized as follows.

- We involve device mobility into the ecosystem of wireless sensing.
- We establish a theoretical model to quantify the effect of device motion on signal variation and accordingly on sensing.
- We propose a novel signal processing scheme to cancel out the device motion induced signal variation to enable sensing in the presence of device motions. The proposed method can be applied to other wideband wireless signals such as FMCW radar signal and acoustic chirp signal.
- We implement Mobi^{2}Sense on commodity UWB hardware and comprehensively evaluate the system performance. We showcase three applications with outstanding performance to demonstrate the effectiveness of our system.

2 PRELIMINARY OF ULTRA-WIDEBAND

In this section, we first introduce the basics of UWB signal and then present traditional sensing model for static transceivers. We then empirically study the effect of device motions on existing wireless sensing applications.

2.1 UWB Primer

The basic concept of UWB transmission is shown in Figure 3. UWB transmitter generates Gaussian pulses $p(\tau)$ modulated on a carrier frequency f_c[1] and the pulse amplitude is V_G. The transmitted signal $x(\tau)$ can be represented as:

$$x(\tau) = V_G \cdot p(\tau) \cdot cos(2\pi f_c \tau). \quad (1)$$

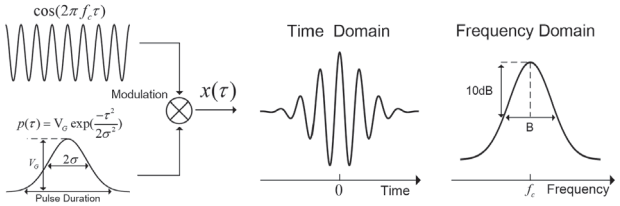

Figure 3: The generation of UWB signal $x(\tau)$.

The transmitted pulse gets reflected back from an object at a time delay of $\tau = \frac{2r}{c}$, where r is the distance between the object and the transceivers, and c is the signal propagation speed in the air. Note that UWB transceivers are co-located. At the receiver side, the received signal is demodulated to the baseband. The pulse signal can get reflected from objects at different distances. These reflections from multiple objects induced by the same pulse form a *frame*. The pulses are transmitted one by one with a certain time interval in between. The frames are ordered in time, forming a 2D-matrix as shown in Figure 4. The X-axis indicates the range bins for one frame and Y-axis indicates time-ordered frames. The X-axis represents the fast time (τ) information and Y-axis represents the slow time (t) information. The fast time information can be used to calculate the distance between the object and the UWB device. Therefore, the matrix is also called *range profile*. The reflection signal from one object can be represented as:

$$y(t) = A \cdot e^{j \cdot 2\pi \cdot f_c \cdot \tau_{ini}}. \quad (2)$$

Here, τ_{ini} is the time delay of the reflection signal and A is the signal amplitude. If the object is moving, causing an extra time delay of $\Delta\tau_{tmov}(t)$, the reflection signal can be represented as:

$$y(t) = A \cdot e^{j \cdot 2\pi \cdot f_c \cdot (\tau_{ini} + \Delta\tau_{tmov}(t))}. \quad (3)$$

We present a range profile example in Figure 5. If a frame has an obvious peak (bright color), it means that there is an object which reflects signal back. The location of the peak at X-axis represents the time delay and accordingly the distance of the object. We divide the X-axis distance into different range bins. The resolution of the range bin is related to the bandwidth of the UWB signal. For example, when the bandwidth (B) is 1.5 GHz, the resolution of the range bin is $c/2B = 10$ cm. In Figure 5, a static object (object 1) is located in the 120th range bin. Another object (object 2) located in the 60th range bin is static in the first 2500 frames (25 s) and moves forward and backward periodically after that. Based on the relationship between the phase change and target displacement $\Delta\phi = 2\pi f_c \Delta\tau_{tmov}(t)$, we are able to sense the target movement information (e.g., displacement and speed) using phase readings.

[1]The allocated frequency bands for UWB are 3.1–10.6 GHz

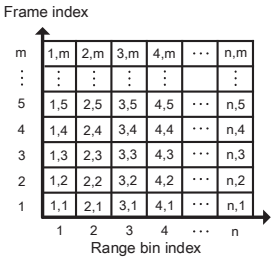

Figure 4: Frame-bin matrix. Range bins present the distance information and frames present the time information.

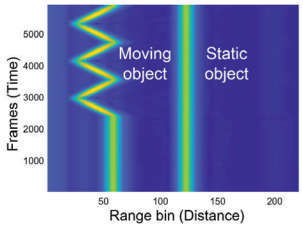

Figure 5: Range profile. The range bins of the moving object change with time while that of the static object remains unchanged.

2.2 Multi-object reflections

In real environment, besides target reflection, other static objects (e.g., furniture and walls) also reflect signals. If we assume there are N reflection paths from static objects in the environment, the reflection path delay of the n-th object is denoted as $\tau_{ini,n}$ and the corresponding reflection signal amplitude is denoted as $A_{ini,n}$, the reflection signal from this object can be written as:

$$y_{s,n} = A_{ini,n} \cdot e^{j \cdot 2\pi \cdot f_c \cdot \tau_{ini,n}} (n = 1, ..., N). \quad (4)$$

Note that signal reflections falling in different range bins can be separated and do not interfere with each other. Here we only consider the case in which the signal reflection from the static object also falls in the same range bin as the target (e.g., the i-th static object). The mixed signal at the target range bin can then be expressed as:

$$y_t(t) = \underbrace{A_{mov} \cdot e^{j \cdot 2\pi \cdot f_c \cdot (\tau_{ini} + \Delta\tau_{tmov}(t))}}_{\text{Dynamic component}} + \underbrace{A_{ini,i} \cdot e^{j \cdot 2\pi \cdot f_c \cdot \tau_{ini,i}}}_{\text{Static component}}, \quad (5)$$

where A_{mov} denotes the amplitude of the signal reflected from the moving target. Note that the signal component reflected from the static object does not change over time and is denoted as static vector (H_s) in the I-Q space. The dynamic vector (H_d) indicates the signal reflected from the moving target. The target movement causes the signal phase to change over time. As shown in Figure 6, when a person sits in a sofa, the reflection from the human body and reflection from the static sofa are located in the same range bin. The received signal $y(t)$ is a superposition of both dynamic and static vectors, and the dynamic vector rotates with respect to the static vector [49]. For a displacement of half-wavelength,[2] the

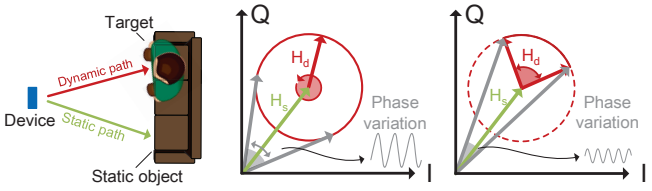

Figure 6: Dynamic signal vector (H_d) rotates with respect to the static signal vector (H_s).

[2]If the central frequency of the UWB signal is 7.3 GHz, half wavelength is 2 cm.

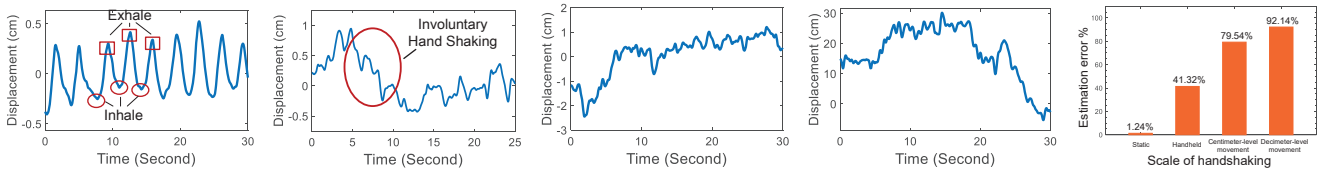

(a) Device is static. (b) Held in hand. (c) cm-level movement. (d) dm-level movement. (e) Respiration rate errors.

Figure 7: Respiration monitoring under different device movement conditions. Clear signal variation pattern corresponding to respiration cycles can be obtained when device is static and device movement corrupts the signal variation pattern.

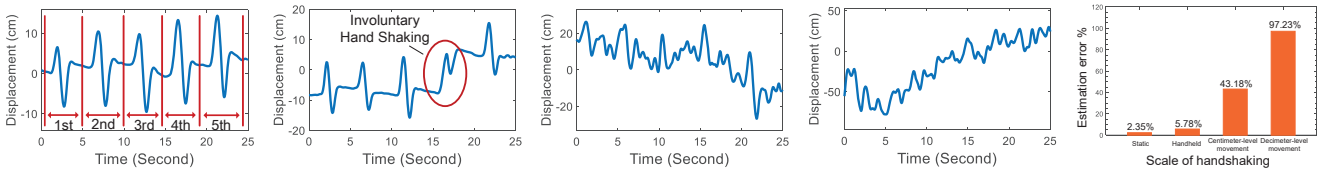

(a) Device is static. (b) Held in hand. (c) cm-level movement. (d) dm-level movement. (e) Displacement errors.

Figure 8: Gesture sensing under different device movement conditions. Clear signal variation pattern corresponding to gestures can be obtained when device is static and device movement corrupts the signal variation pattern.

dynamic vector rotates for 360°. For a subtle chest displacement of 0.5 cm for respiration, the dynamic vector rotates for around 87°. Note that for a small movement such as respiration, the amplitude of the dynamic signal can be considered as a constant. In contrast, the phase change is large (87°) which can not be ignored.

2.3 Wireless sensing under device motions

Based on the analysis in Section 2.2, if an RF device is static, the phase change induced by target movement can directly be used to obtain the target movement information. We take two typical sensing applications, i.e., respiration monitoring and gesture recognition as the examples. As shown in Figure 7a, clear periodic signal variation corresponds to the exhalation and inhalation of human breathing. In Figure 8a, the user draws a "triangle" in the air five times using his hand and we can clearly see the repeated pattern of each drawing.

Now we study the impact of device motion on the two sensing applications. As shown in Figure 7b, for respiration monitoring, when the device is held in hand without any intentional movements, the signal pattern is still corrupted by the subtle involuntary hand shaking. We further increase the motion scale of the device. In Figure 7c and 7d, centimeter and decimeter level of device motions completely corrupt the breathing pattern. In Figure 7e, we show the average error of respiration rate estimation when the device is static and in the presence of different scales of movements. The ground truth is measured by a respiration monitor belt logger sensor NUL-236 [9]. We can see that when the device is static, the error is as low as 1.24% in terms of respiration rate. In handheld scenario, involuntary hand movements lead to a significant increase of estimation error from 1.24% to 41.32%. Large-scale centimeter and decimeter movements further increase the error to 79.54% and 92.14%, respectively.

For in-air gesture recognition, the gesture movements are performed with a large displacement of around 10 cm. For handheld scenario, as shown in Figure 8b, involuntary handheld motion induces a notable signal variation at the 17th second but we can still observe the clear signal pattern of the gesture. When the hand movement is larger, the signal pattern of gesture is seriously corrupted as shown in Figure 8c and 8d. In Figure 8e, we show the average error of displacement measurement.[3] The ground truth is captured by HTC ViVe tracking system [11]. We can see that when the device is held in hand with involuntary shaking, the displacement estimation error is 5.78%. With centimeter and decimeter level hand movements, the displacement estimation error of gesture increases to 43.18% and 97.23%, respectively. From these results, we can see that device motions can severely affect the performance of wireless sensing. Exiting wireless sensing systems do not work in the presence of device motions.

3 UNDERSTANDING THE EFFECT OF DEVICE MOTION ON SENSING

In this section, we first model the effect of device motion on target-reflection signal and static signal, respectively. Then we present the proposed scheme to cancel out the effect of device motion to enable sensing.

3.1 Modeling target signal in the presence of device motion

We now take device motion into consideration. Besides target movement $\Delta\tau_{tmov}(t)$ in Equation 5, the device movement $\Delta\tau_{dmov}(t)$ is also introduced, which can be from a hand holding the device or a robot carrying the device. Thus, the signal reflected from the target contains movement information of both target and device. The received signal at the target range bin can thus be represented

[3]The displacement error in percentage is calculated as the ratio of the measured displacement error and the ground truth displacement, which may exceed 100%.

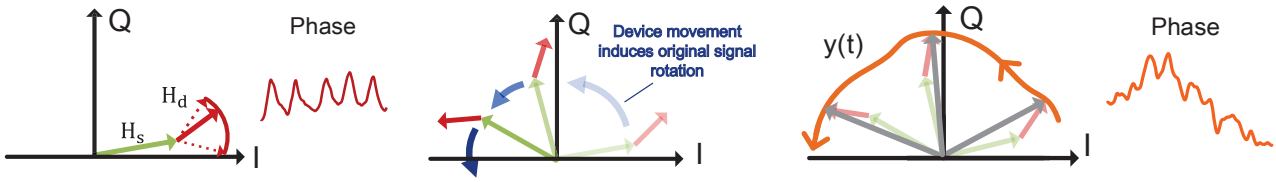

(a) Signal phase change due to target motion. (b) The effect of device motion. (c) Signal phase change in the presence of device motion.

Figure 9: Modeling the effect of device motion on signal variation and accordingly on sensing.

as:

$$y(t) = A_{mov} \cdot e^{j\cdot 2\pi\cdot f_c\cdot(\tau_{ini}+\Delta\tau_{dmov}(t)+\Delta\tau_{tmov}(t))} + A_{ini,i} \cdot e^{j\cdot 2\pi\cdot f_c\cdot(\tau_{ini,i}+\Delta\tau_{dmov}(t))}. \quad (6)$$

Both dynamic and static vectors contain $e^{j\cdot 2\pi\cdot f_c\cdot\Delta\tau_{dmov}(t)}$, that is, the phase shift caused by device motion. Let H_t denote $A_{mov}\cdot e^{j\cdot 2\pi\cdot f_c\cdot(\Delta\tau_{tmov}(t)+\tau_{ini})}$, which is the dynamic vector induced by target movement without device motion, and $H_{s,i}$ denote $A_{ini,i}\cdot e^{j\cdot 2\pi\cdot f_c\cdot\tau_{ini,i}}$, which is the static vector induced by the i-th static object in the same range bin without device motion. We extract the common term related to device motion out and the formula can be rewritten as:

$$y(t) = \boxed{e^{j\cdot 2\pi\cdot f_c\cdot\Delta\tau_{dmov}(t)}}\cdot(H_t + H_{s,i}). \quad (7)$$

The term $e^{j\cdot 2\pi\cdot f_c\cdot\Delta\tau_{dmov}(t)}$ represents the effect of device motion on signal. It rotates the original static and dynamic vectors on the complex I-Q plane together by a phase of $2\pi\cdot f_c\cdot\Delta\tau_{dmov}(t)$, as shown in Figure 9b. This explains the fundamental effect of the device motion on signal variation and accordingly on sensing. Specifically, when the device moves, the original static vector and dynamic vector rotate together. The device motion induced signal variation can submerge the target motion induced signal variation, and the overall phase variation mainly reflects the device movements as shown in Figure 9c. Therefore, the effect of device motion is mixed with the effect of target movement and the original phase variation is severely distorted in the presence of device motions.

3.2 Modeling static object signals in the presence of device motion

When an RF device moves, the signals reflected from static objects in the environment also contain the device motion information. Assuming there are N static objects in the environment which reflect signal, the extra delay introduced by device motion at the n-th reflection is denoted as $\Delta\tau_{dmov,n}(t)$. Note that objects exhibit different delays due to different relative positions with respect to the device. Signal reflection from static objects contains only device motion information:

$$y_{s,n}(t) = A_{ini,n}\cdot\boxed{e^{j\cdot 2\pi\cdot f_c\cdot\Delta\tau_{dmov,n}(t)}}\cdot e^{j\cdot 2\pi\cdot f_c\cdot\tau_{ini,n}} = \boxed{e^{j\cdot 2\pi\cdot f_c\cdot\Delta\tau_{dmov,n}(t)}}\cdot H_{s,n}(n=1,...,N). \quad (8)$$

Here $H_{s,n} = A_{ini,n}\cdot e^{j\cdot 2\pi\cdot f_c\cdot\tau_{ini,n}}$ is used to denote the signal reflection from the n-th static object without the effect of device motion.

3.3 Device motion cancellation

Now we know that target reflection contains both device and target movement information, whereas the reflections from static objects contain only the device movement information. Intuitively, a straightforward method to deal with device motion is to remove the device motion effect by subtracting the static reflection signal from the target reflection signal similar to interference cancellation [37, 43]. However, we quickly realize this is not correct because the movement effect does not bring in a new signal but just causes the existing signal to vary. Therefore, subtracting signal does not work and we need a more delicate scheme to remove the effect induced by device motions.

By deeply understanding the effect of device motion which is an extra amount of phase change[4] applied to both original static signal and dynamic signal, we propose to cancel out the effect of device motion through a division operation between target-reflection signal and one static object-reflection signal (e.g., the reflection from the k-th static object):

$$y_{new}(t) = \frac{y_t(t)}{y_{s,k}(t)} = \frac{\boxed{e^{j\cdot 2\pi\cdot f_c\cdot\Delta\tau_{dmov}(t)}}\cdot(H_t + H_{s,i})}{\boxed{e^{j\cdot 2\pi\cdot f_c\cdot\Delta\tau_{dmov,k}(t)}}\cdot H_{s,k}}. \quad (9)$$

However, the two terms $\Delta\tau_{dmov}(t)$ $\Delta\tau_{dmov,k}(t)$ are not exactly the same and they can not be cancelled out. This is because device movement is a relative information related to the reflector's location. As the target and the static object are not located at the same position, the movement induced signal phase changes are not the same. We therefore need to convert the motion effect (signal change) at the static object location to that at the target location so they can be cancelled out. This is a non-trivial task because it requires to know the target and static object's precise location information. In this work, we propose a search-based scheme to quickly identify the correct conversion to cancel out the device motion effect without requiring to know the physical location of the target and the static object. We present the detailed design in Section 4.2.

4 MOBI^{2}SENSE DESIGN

In this section, we introduce the detailed design of our system. Figure 10 shows the workflow of Mobi^{2}Sense, which consists of three core modules.

- **Reference selection.** Our key idea is to select a static object as the reference to cancel out the effect of device motion. There are usually multiple static objects we can select from in the environment. Different static objects can present us different cancellation

[4]Note that the signal amplitude can be considered as a constant within a small time window.

effects and therefore we need to select the most appropriate one for motion cancellation.

- **Device motion cancellation.** After the reference is selected, we proceed to cancel out the effect of device motion. As the target and reference object are located at different positions, effects of device motion on them are also different. Therefore, a delicate motion effect conversion needs to be performed before the effect of device motion can be successfully cancelled out.
- **Target movement recovery.** After the effect of device motion is cancelled out, the remaining target reflection signal contains only the target motion. However, note that the motion cancellation step only removes the effect of device motion, the reflection signals from close-by static objects can still exist, superimposed with target reflection in the same range bin. Although static reflections do not change, the superimposition still alters the phase/amplitude variation of target reflection signal and therefore needs to be removed before we can obtain accurate target information.

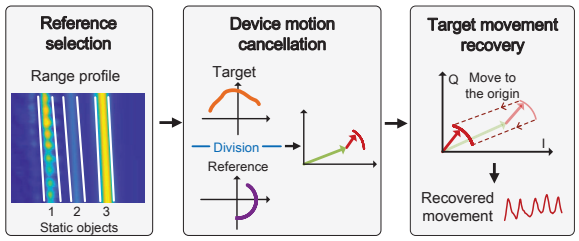

Figure 10: Overview of Mobi^{2}Sense.

4.1 Reference selection

In reality, there are usually multiple static objects available. To achieve the best performance of device motion cancellation, we need to select the one with the best signal quality as the reference. The suitability of a static object as a reference is measured based on the signal strength and stability. This is because more accurate device motion information can be obtained from a strong and stable signal. To take both factors into consideration, we use the ratio of the signal strength and variance as the selection criterion. Note that we keep a list of available static objects which can be used as a reference. If the selected static object has moved, we choose another one from the remaining static objects on the list as the reference. Also as the device is moving, the static objects on the list also change and our system updates the list accordingly.

4.2 Device motion cancellation

After reference selection, we proceed to eliminate device motion. However, device motion can not be easily removed because the effect caused by device motion at the reference is not the same as that at the target. To understand this, we analyze the signal variation induced by device motion at the target and at the reference respectively. As shown in Figure 11a, there are two objects in the environment, one is a static chair and the other is a human target. The angle between the device motion direction and the two objects' locations are denoted as θ_r and θ_t, respectively. Assume that in a short time interval, the device displacement is Δd. Accordingly, we can obtain the path length change of the signal from the device to the two objects as ΔL_r and ΔL_t, respectively. Based on simple triangle geometry, we can obtain the following relationship: $\Delta L_r = \Delta d \cdot cos\theta_r$ and $\Delta L_t = \Delta d \cdot cos\theta_t$. The device motion induced signal phase changes at the two objects can then be calculated as $\Delta\phi_r = 2\pi f_c 2\Delta L_r/c$ and $\Delta\phi_t = 2\pi f_c 2\Delta L_t/c$. When $\theta_r \neq \theta_t$, the phase changes are also different. In this case, the division operation between the target reflection and static object reflection in Equation 9 can not cancel out the effect of device motion.

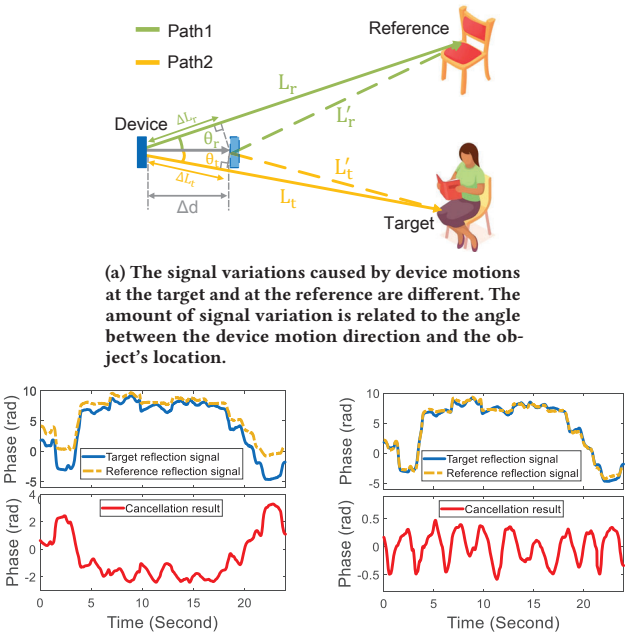

(a) The signal variations caused by device motions at the target and at the reference are different. The amount of signal variation is related to the angle between the device motion direction and the object's location.

(b) Direct division operation between target reflection and reference reflection can not cancel out the effect of device motion. The respiration pattern can not be clearly visualized.

(c) After applying the compensation coefficient to make device-induced phase variation consistent at the target and at the reference, the effect of device motion is cancelled out.

Figure 11: The effect of applying a proper compensation coefficient for device motion cancellation.

If the direction information of the two objects with respect to the device (θ_r and θ_t) can be obtained, we can compensate the difference by simply multiplying the phase change induced by device motion at the static object with $\Delta\phi_t/\Delta\phi_r$ to obtain the phase change at the target. However, to achieve a clean cancellation, highly accurate angle information is needed and a large antenna array is required. From our empirical studies, an 8-antenna array is still far away from achieving the required level of angle estimation accuracy. Therefore, in this paper, we propose a search-based solution which is able to achieve highly accurate device motion cancellation without a need to measure accurate angle information of the reflection signals. We define the required compensation coefficient β which needs to be applied for device motion cancellation below:

$$\beta = \frac{\Delta\phi_t}{\Delta\phi_r} = \frac{\Delta L_t}{\Delta L_r} = \frac{\Delta d \cdot cos\theta_t}{\Delta d \cdot cos\theta_r} = \frac{cos\theta_t}{cos\theta_r}. \quad (10)$$

By applying this compensation coefficient, we transfer the device-induced phase variation at the reference to the phase change at the target. Then the device-induced phase variation can be cancelled out. So the key is to obtain the compensation coefficient β. From Equation 10, we know that β is dependent on the device movement

direction. The device movement direction can be assumed as a constant in a small time window. Let Pr_n and Pt_n denote the phase of the n-th signal samples of reference reflection and target reflection respectively. The total number of signal samples is N. To search the optimal β in each time interval, we optimize the following function:

$$\arg\min_{\beta,\gamma} \sum_{n=1}^{N} ((\beta \cdot Pr_n + \gamma) - Pt_n)^2. \tag{11}$$

Here γ is a constant phase value which helps move the phases of all the samples up/down. This function finds a β which can minimize the difference between the phase of the reference reflection and target reflection after compensation. This optimization problem can be solved by the least square algorithm [33] to obtain the optimal β value. The rationale behind this optimization is that the two phase curves are closest in this time interval, as shown in Figure 11c. Note that for a small device motion, β does not change much and therefore it can be assumed as a constant in a large time window. For a large device motion, we need to update β more often.

By applying the compensation coefficient β, we make $\Delta\tau_{dmov}(t) = \beta \cdot \Delta\tau_{dmov,k}(t)$ in Equation 9. The phase of $H_{s,k}$ is also multiplied by β and it changes to $H'_{s,k} = A_{ini,k} \cdot e^{j\cdot 2\pi \cdot f_c \cdot \beta \cdot \tau_{ini,k}}$, which is still a static component. We thus can eliminate the signal phase change $e^{j\cdot 2\pi \cdot f_c \cdot \Delta\tau_{dmov}(t)}$ caused by the device motion. The detailed derivation process is as follows:

$$\begin{aligned} y_{new}(t) &= \frac{y_t(t)}{y'_{s,k}(t)} = \frac{\boxed{e^{j\cdot 2\pi \cdot f_c \cdot \Delta\tau_{dmov}(t)}} \cdot (H_t + H_{s,i})}{\boxed{e^{j\cdot 2\pi \cdot f_c \cdot \beta \cdot \Delta\tau_{dmov,k}(t)}} \cdot H'_{s,k}} \\ &= \underbrace{A'_{mov} \cdot e^{j\cdot 2\pi \cdot f_c \cdot (\Delta\tau_{tmov}(t) + \tau_{ini} - \beta \cdot \tau_{ini,k})}}_{\text{New dynamic component}} + \underbrace{A'_{ini} \cdot e^{j\cdot 2\pi \cdot (f_c \cdot \tau_{ini} - \beta \cdot \tau_{ini,k})}}_{\text{New static component}}, \end{aligned} \tag{12}$$

where A'_{mov} and A'_{ini} are the amplitude of new dynamic component and new static component, respectively. Note that τ_{ini} and $\tau_{ini,k}$ are constants related to object position. The obtained new signal only contains $\Delta\tau_{tmov}(t)$ which is the target motion induced phase variation.

4.3 Target movement recovery

After we cancel out the effect of device motion, we obtain clean phase change induced by target movement. However, besides the target reflection, reflections from close-by static objects may exist. Different from those reflections from static objects far away, the reflection from close-by objects can fall in the same range bin as the target reflection and therefore can not be easily separated. The static signal needs to be removed before we can obtain accurate target movement information. We use an example in Figure 12 to illustrate the concept. We can see that the dynamic signal rotates an angle of $\Delta\varphi$. However, if the static signal is not removed, the phase change we obtain from the composite signal is $\Delta\varphi'$, which is much smaller than $\Delta\varphi$. Note that the amount of phase rotation is critical in calculating target displacement.

We estimate the static vector through circle fitting [27]. The rationale is that the amplitude of the dynamic signal can be considered as a constant for fine-grained movements such as gesture or respiration. Take respiration as the example, the chest displacement is just around 5 mm. This displacement causes roughly a signal

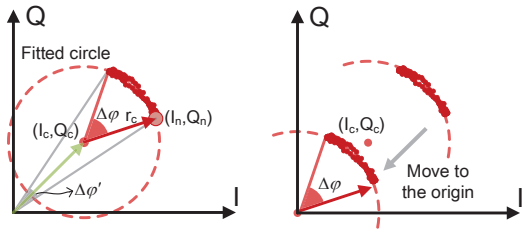

Figure 12: Illustration of circle fitting and static vector removal.

path length change of 10 mm. Compared to a target-device distance of 2 m, this 10 mm distance change only causes the amplitude to vary by around 0.5%. On the other hand, a 5 mm displacement can cause a large phase change of 87°. Therefore, during the movement process, the dynamic vector rotates with respect to the static vector, forming a circle. The circle radius indicates the amplitude of the dynamic vector. We can then leverage this circle property to calculate and remove the static signal [42]. We regard the circle fitting as the best linear unbiased estimates of arc center (I_c, Q_c) and radius r_c [42]. The arc can be estimated as $[\hat{I}_c, \hat{Q}_c, \hat{\psi}]^T = (\boldsymbol{H}^T\boldsymbol{H})^{-1}\boldsymbol{H}^T\boldsymbol{Y}$, where

$$\boldsymbol{H} = \begin{bmatrix} 2I_1 & 2Q_1 & 1 \\ 2I_2 & 2Q_2 & 1 \\ \vdots & \vdots & \vdots \\ 2I_N & 2Q_N & 1 \end{bmatrix}, \boldsymbol{Y} = \begin{bmatrix} I_1^2 + Q_1^2 \\ I_2^2 + Q_2^2 \\ \vdots \\ I_N^2 + Q_N^2 \end{bmatrix}, \tag{13}$$

(I_n, Q_n) is the coordinate of the n-th sample in the complex plane, N is the total number of samples, and $\hat{\psi} = \hat{r_c}^2 - \hat{I_c}^2 - \hat{Q_c}^2$. After we obtain the static vector, we remove it from the received signal to obtain the clean target reflection signal. We move the center of the dynamic vector to the origin on the complex plane. We can then obtain correct target movement distance by calculating the phase change of the signal only reflected from target.

5 IMPLEMENTATION

Hardware Implementations. We implement Mobi^{2}Sense on a COTS UWB hardware (XETHRU X4M05) which has an integrated X4 system-on-chip [16]. X4M05 chip works on the 7.25–10.2 GHz frequency band. The unit cost of the XETHRU X4M05 is $249 and the price can drop to $80 for bulk purchase [4]. It integrates two on-board antennas embedded onto a 6.6 × 4.2 cm^2 PCB board. Benefit from its high-speed analog-to-digital module, the raw sampling rate is 23.328 GS/s. The data processing happens on a Dell XPS-15 9570 laptop with an Intel i7-8750H processor and 16GB memory. The UWB chip [7] has a much lower power consumption (0.084 mW) compared to WiFi and RFID chips. We connect the UWB module to the Raspberry Pi and package it in a 3D-printed box with a size of 13.9 × 9.4 cm^2 as a handheld sensing device as shown in Figure 13.[5] We use a commercial Reeman mobile robot [40] to move the UWB device as a mobile sensing platform. We use Python to control robot movement (i.e., moving speed, direction and distance).

Software Implementations. We implement the signal processing on Matlab. After the Raspberry Pi receives the raw signal

[5]The UWB module size can be further reduced using Wafer Level Chip Scale Packaging (WLCSP). This design has been adopted in Lenovo X1 laptop.

samples from the UWB module, it forwards the raw data to the laptop through WiFi connection. We restructure the raw data into a matrix form to obtain the range profile as illustrated in Figure 5. Then we perform signal phase compensation and eliminate the effect of device motion using a reference.

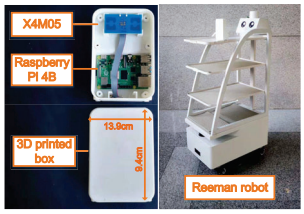

Figure 13: Hardware implementation.

Figure 14: Setup of benchmark experiment.

6 EVALUATION

In this section, we evaluate the sensing performance of the system using both benchmark experiments and real-world applications. Benchmark experiments are employed to verify the effectiveness of the proposed schemes and study the influence of varying parameters and conditions. We showcase three sensing applications with the proposed system: i) sensing sub-millimeter level vibration of a speaker to "hear" the music play; ii) holding the UWB device in hand to monitor the patients' millimeter level respiration (rate and depth) in a hospital environment; and iii) placing the UWB device on a moving robot to recognize gestures of multiple persons.

6.1 Benchmark experiment

Experiment Setting: As shown in Figure 14, we use a metal plate which is an ideal signal reflector as the target[6] in this benchmark experiment. The metal plate has a size of 10×15 cm^2 and we employ a 2 m-long sliding track controlled by Raspberry Pi 3 Model to precisely move the metal plate. We use another stationary metal plate as the reference to eliminate the device motion. We also consider commonly-seen static objects as reference in Section 6.1.4. The default moving speed of the robot is 0.2 m/s.

Ground Truth: We move the target with a high-precision sliding track (Mjunit MJ45N) which is capable of achieving an accuracy of 0.01 mm.

Performance metric: We use the mean absolute error between the displacement estimated by our system and ground truth as the metric to evaluate the system performance.

6.1.1 ***How effective can device motion of different scales be addressed?*** We first investigate the impact of device motion scale on our system. We let the target move periodically for 1 cm on the sliding track. When the RF device is held in hand by a person, we observe that even the person keeps still, the subtle involuntary hand shaking can cause a hand movement around 0.2-0.5 cm.[7] As shown in Figure 15, if the device motion is not removed, the involuntary shaking causes a large error of 0.34 cm. When the involuntary shaking is cancelled out using the proposed method, the average error is reduced to 0.02 cm. We further ask the user to intentionally shake the hand with a gradually increasing scale from 1 cm to 5 cm. In this case, the target movement is completely submerged by hand movement. We can see that if the device motion is not addressed, the error of displacement estimate increases from 0.52 cm to 2.73 cm. In contrast, by applying the proposed device motion cancellation method, the error is reduced to below 0.08 cm.

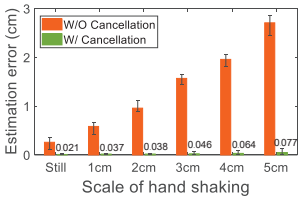

Figure 15: Effect of hand shaking scale.

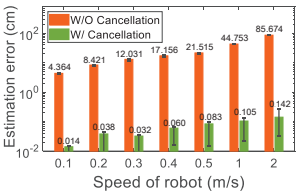

Figure 16: Effect of robot moving speed.

6.1.2 ***How effective can device motion of different speeds and trajectories be addressed?*** We further explore the impact of motion speed on the performance of our system. We move a robot for 1 m which is much larger than the hand movement scale in the previous experiment. We increase the robot speed from 0.1 m/s to 2 m/s. As shown in Figure 16, we can see that the device movement speed does affect the sensing performance. Without the proposed method, the error can be up to 85.67 cm at 2 m/s. With the proposed method, for all seven speeds, the displacement estimation errors are below 0.15 cm.

We also study the impact of different moving trajectories of the robot. As shown in Figure 17a and 17b, we let the robot cruise following five different trajectories including (1) a horizontal line, (2) a vertical line, (3) a diagonal line, (4) a horizontal Z shape and (5) and a vertical Z shape. For five different trajectories, the estimation errors are 0.04 cm, 0.06 cm, 0.10 cm, 0.12 cm and 0.06 cm, respectively, demonstrating a high accuracy under different robot moving trajectories.

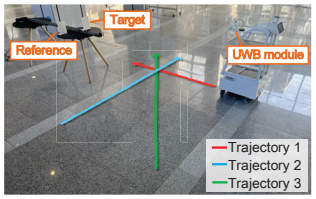

(a) Straight line trajectories.

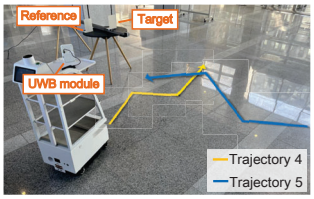

(b) "Z" shape trajectories.

Figure 17: Robot moves following different trajectories.

6.1.3 ***Robot's moving direction is parallel to the wall.*** When the robot's moving direction is parallel to the wall as shown in Figure 18a, the wall cannot be used as a reference because the distance between the device and the wall is a constant and does not contain device motion information. Fortunately, our system can detect the parallel wall and exclude it from being selected as a reference. As shown in the range profile in Figure 18b, the distance

[6]Experiments with human target will be presented in the application section.

[7]The displacement of subtle handshaking is measured by the Qualisys motion capture camera system[12], which can achieve a sub-mm level accuracy. Four ultra high-speed cameras are mounted on the wall at a height of 2.8 m. The frame rate of the Qualisys system is set as 250 Hz. A reflective marker needs to be attached to the the target for Qualisys MoCap system to work.

of the parallel wall is roughly a constant over time. The parallel wall can thus be detected and excluded from being considered as the reference for device motion cancellation. By selecting the small metal plate on the desk as the reference, target motion can be recovered as shown in Figure 18c.

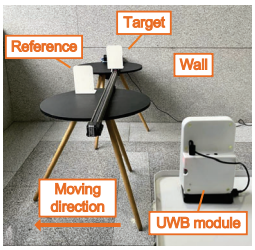

(a) Experiment setup.

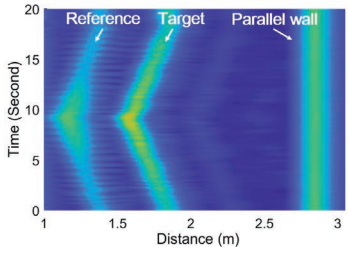

(b) Range-time profile.

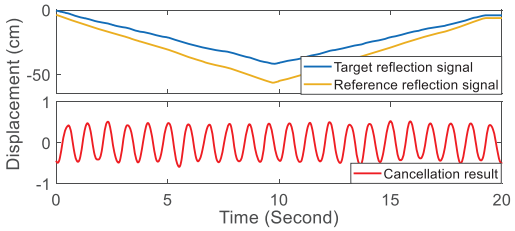

(c) Device motion removal using the metal plate as reference

Figure 18: Experiment setup and device motion removal. When the robot moves in parallel with the wall, the wall is excluded from being selected and the small metal plate is selected as the reference.

6.1.4 ***Effect of selecting different static objects as the reference.*** Many commonly seen static objects can be selected as reference to eliminate the influence of device motion. We therefore conduct experiments to evaluate the effect of selecting different static objects in real environment as the reference. We employ eight commonly seen static objects, i.e., water bottle, bookshelf, chair, table, bookcase, laptop, sofa and wall in two scenarios, as shown in Figure 19a and 19b as the reference. We let the target move periodically for 1 cm on the sliding track. In each scenario, we evaluate the displacement tracking accuracy in both handheld and robot-carried scenarios. The results are presented in Figure 20a and 20b. We can see that all the static objects in the range can be chosen as reference to successfully cancel out the device motion. We can also see that a larger error occurs when sofa is chosen as the reference. This is because sofa is far away and the clothe surface is not as smooth as other objects so the signal reflection is weaker.

6.1.5 ***Challenging real-life scenarios.*** We now evaluate the system performance in challenging real-life scenarios. When device is held in hand, we consider two cases: i) the user changes the hand to hold the device and ii) the user holds the device and walks. For robot case, we let the robot move on four rough grounds: carpet, steel, brick, and soil as shown in Figure 21b. We show the performance of sensing a target with a small 1 cm displacement in these challenging scenarios. It can be seen that without the proposed motion cancellation scheme, the average target motion displacement

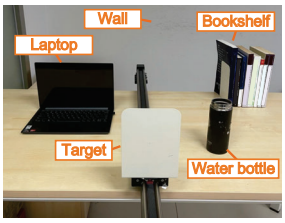

(a) Desk scenario.

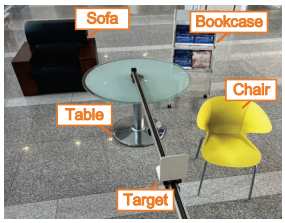

(b) Lobby area scenario.

Figure 19: A lot of commonly seen objects in our environment can be selected as reference for device motion removal.

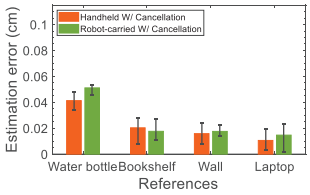

(a) The result of selecting different objects on the desk as the reference.

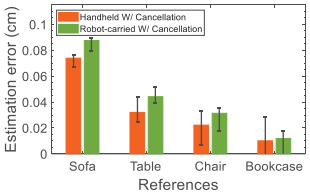

(b) The result of selecting different objects in the lobby area as the reference.

Figure 20: The effect of selecting different commonly seen object in our surrounding environment as references.

error reaches 8.87 cm, 15.52 cm, 13.81 cm, 14.27 cm, 16.45 cm and 16.98 cm respectively. In contrast, with the proposed method, the displacement error is reduced dramatically to below 0.31 cm for all six challenging scenarios.

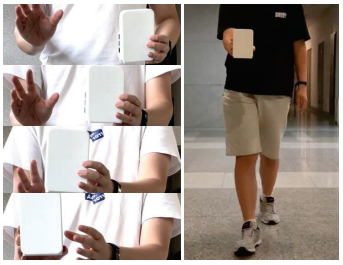

(a) Change the hand holding the device.

(b) Robot moves on rough ground.

Figure 21: Challenging real-life scenarios.

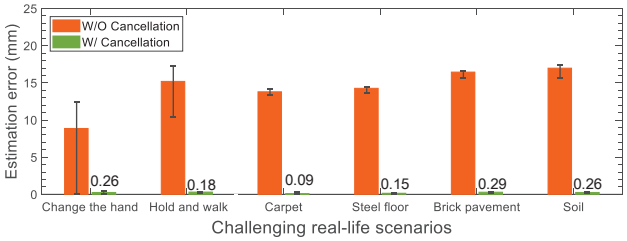

Figure 22: The performance of fine-grained sensing, i.e., tracking a target displacement of 1 cm in the six challenging real-life scenarios.

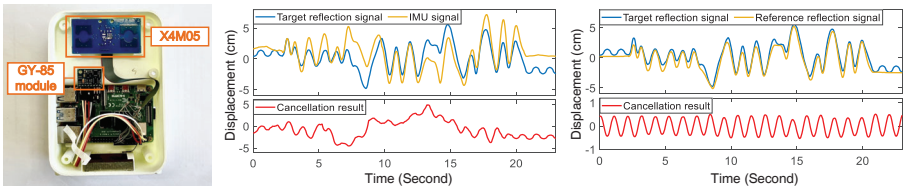

(a) GY-85 IMU module. (b) IMU-based device motion removal. (c) The proposed device motion removal.

Figure 23: Performance comparison between IMU-based and the proposed reference-based device motion removal methods.

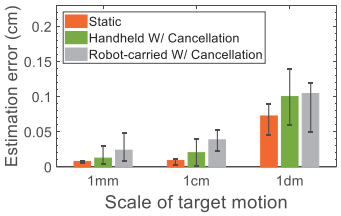

Figure 24: Performance comparison with static device scenario.

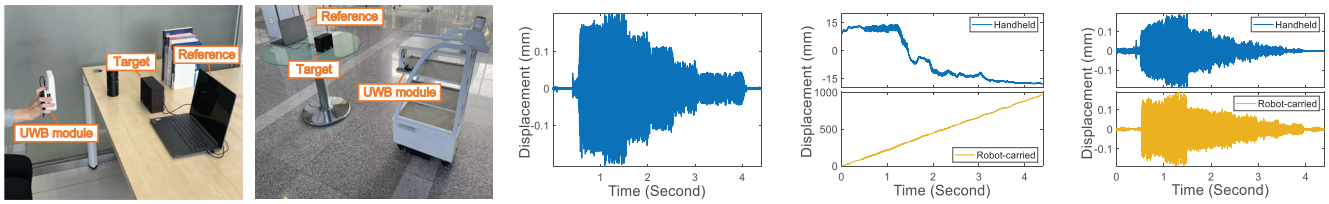

(a) Handheld scenario. (b) Robot-carried scenario. (c) Ground truth signal captured by static device. (d) Sensing signal corrupted by device motions. (e) Recovered signal.

Figure 25: The experiment setups and the results of sensing fine-grained speaker vibrations.

6.1.6 ***Performance comparison with IMU-based cancellation.*** In this section, we compare the system performance with IMU-based device motion cancellation. To make IMU and UWB work together, we use a Raspberry Pi to connect a high-end 9-axis IMU sensor (GY-85 module) and our X4M05 UWB as shown in Figure 23a. We record the IMU and UWB data with timestamps for time synchronization. Acceleration information can be obtained from the IMU sensor and we convert it to displacement through the integration operation. For a fair comparison, we apply the same method proposed in this work to cancel the target motion using the IMU data and UWB-reference data respectively. The results are shown in Figure 23b and Figure 23c. We can see that while IMU data can be used to cancel the device motion, it is not as accurate as the UWB-reference based method.

We further compare the performance of our system with a static device. As shown in Figure 24, in both handheld and robot-carried scenarios, the achieved performance is close to that achieved with a static UWB device. These results demonstrate the effectiveness of the proposed scheme in dealing with device motions.

6.2 Case studies

We conduct case studies to evaluate the performance of Mobi^{2}Sense in real-life applications.

6.2.1 ***"Listen to" music through fine-grained UWB sensing.*** In this application, we demonstrate Mobi^{2}Sense can be used to "listen to" music through wireless sensing. In this experiment, we use our system to sense the sub-millimeter level vibration of a commodity speaker (Philips SPA20) when it is playing music. The sampling rate of the UWB system is set to 1200 samples/s. We conduct experiments in two scenarios as shown in Figure 25a and 25b in which the devices are handheld and robot-carried, respectively. The speaker is placed on the desk. There are other static objects (i.e., water bottle, laptop and bookshelf) on the desk. The selected reference is the laptop. We play the seven basic music notes, i.e., do, re, mi, fa, so, la and si with the frequency ranges from 261 Hz to 494 Hz and a song *Twinkle twinkle little star*. Because the speaker vibrates when playing music, we can sense the fine-grained vibration information of the speaker and recover the sound the speaker is playing purely through wireless sensing. This technology can be applied to snoop sound or record sound in a noisy environment.

As shown in Figure 25c, we present the ground truth music waveform, which is the music waveform captured by our system when the device is static. Figure 25d and Figure 25e show the corrupted music waveform when the device is mobile and the recovered waveform by applying our motion removal technique, respectively. We can clearly see that our system can hear the music through fine-grained vibration sensing and our system can recover the very subtle vibration information in the presence of hand and robot motions. The demo video can be found at https://youtu.be/0IfiomQ9Jnw.

6.2.2 ***Respiration rate and depth sensing.*** Next, we show the feasibility of using Mobi^{2}Sense to monitor fine-grained human respiration (millimeter level). Vital sign sensing plays a key role in health care. We show that our proposed system can enable the nurse to hand hold the device to sense the patient's respiration. The UWB device can also be placed on a robot to patrol around to monitor the human vital signs.

In the first scenario, the patients lie in bed and breath normally. As shown in Figure 26a, a nurse holds our UWB device in hand 1 m away from the patient to monitor the respiration. A lot of static reflectors in the hospital room can be chosen as reference including bed, bedside desk and wall. The selected reference is the bedside desk. In the second scenario as shown in Figure 26b, as the robot moves, the distance between the device and the human target is between 2-5.5 m. The selected reference is the laptop. Figure 26c

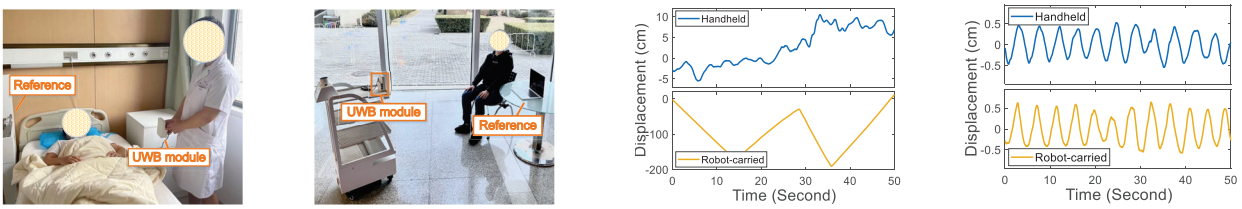

(a) Handheld scenario. (b) Robot-carried scenario. (c) Signal corrupted by device motions. (d) Recovered signal.

Figure 26: The experiment setups and the results of sensing human respiration.

and Figure 26d show the original signal phase variation corrupted by the device motion and the recovered phase variation respectively during the respiration process. We can clearly see that the signal phase variation pattern is severely corrupted by device motions.

To verify the robustness of the system, in the first scenario, we recruit 10 patients with IRB approval. The ground truth is measured by a professional three-lead electrocardiogram monitor (HealForce PC-3000) which costs around $1000 [5]. Note that most wireless sensing-based respiration monitoring systems [9] only pay attention to respiration rate. Owing to our static signal removal scheme presented in Section 4.3, we are able to obtain not just the respiration rate but also the depth. Figure 27a and Figure 27b show the CDF plots of respiration rate estimation error and respiration depth estimation error. Our system achieves a mean respiration rate error below 0.1 bpm (Breaths Per Minute) which is much lower than the 1 bpm requirement for respiration sensing. The mean depth estimation error is below 2 mm.

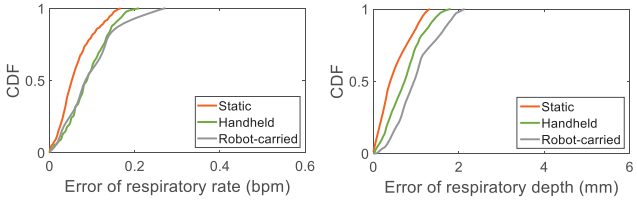

(a) Respiration rate error. (b) Respiration depth error.

Figure 27: Performance comparison when the device is static and and when the device is mobile.

6.2.3 ***"Recognize" multi-target gestures*** . We employ Mobi^{2}Sense to recognize human gestures while the robot is moving. As shown in Figure 28, four commonly-seen hand gestures are employed in this experiment: 1) push, 2) zig-zag, 3) triangle and 4) circle. Note that the gestures which can be supported by our system are not limited to these four. The repetition for each gesture is ten. We let the robot move following the five trajectories shown in Figure 17. The distance between the robot and target is 2-7 m as the robot moves. The chair is selected as the reference.

We first let one target perform each gesture when robot is moving. We can see in Figure 29 that the signal variations are clearly different for the four gestures. We apply the simple dynamic time warping (DTW) method to recognize the gestures. When there is

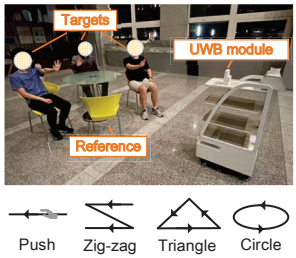

Figure 28: The experiment scenario for multi-target gesture recognition.

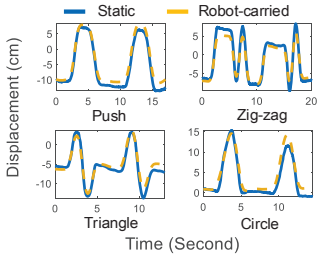

Figure 29: Signal patterns of four gestures. Each gesture is repeated twice.

one target, the confusion matrix is shown in Figure 30a. We can see that even when the device moves with robot, we can achieve a 100% accuracy.

With a large signal bandwidth, the spatial resolution of UWB sensing is high and the proposed system has the capability to sense multiple close-by targets. In Figure 28, we further let three targets sitting around a table perform gestures simultaneously while the robot is moving. Even with multiple targets interfering with each other, the gesture recognition accuracy is still higher than 90% as shown in Figure 30b. Another interesting observation worth mentioning is that for gesture recognition, we can even employ the human body as the reference to eliminate device motion for sensing.

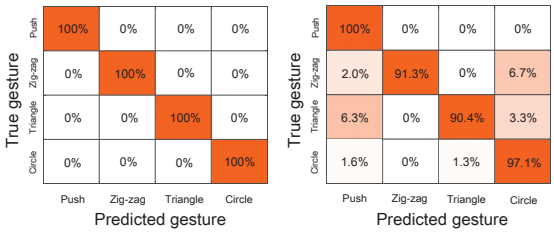

(a) Single target. (b) Multiple targets.

Figure 30: Confusion matrices of gesture recognition.

7 RELATED WORK

Contactless sensing using various RF signals: Research efforts have been devoted to sensing human and objects in a contactless

manner. A large variety of wireless technologies are utilized for sensing including WiFi [15, 54, 60], RFID [46], LoRa [18, 63, 64], LTE [19, 35], FMCW radar [69, 70] and UWB [24, 71, 72]. Among these technologies, WiFi has attracted a lot of research attention due to its pervasiveness and low cost. However, the narrow bandwidth limits the sensing accuracy of WiFi. Another critical issue with WiFi sensing is that it is not compatible with WiFi communication. In contrast, UWB technology has a large bandwidth and can be dedicated for ranging and sensing purposes.

Wireless sensing applications: Wireless sensing has been applied to sense human targets, objects, and also the environment. A large range of sensing applications have been developed ranging from vital sign monitoring [51, 59, 61, 68], gesture tracking [3, 38], daily activity recognition [31, 66] and passive localization [13, 14, 47] to machine vibration sensing [6, 57], food quality monitoring [39], material sensing [55], liquid identification [30], temperature sensing [17, 65] and soil moisture monitoring [18]. We envision that mobility can further expand the application scope of wireless sensing to realize more exciting sensing applications.

Ultra-wideband (UWB) based sensing: In 2002, the FCC released regulations on the use of spectrum and power for civilian UWB technology [1]. UWB technology has then been mainly used for high-precision positioning [50, 74]. Recent research works utilize UWB for contactless sensing [23, 24, 34, 72]. Multi-Breath [58] employs UWB for human respiration sensing, which can support up to four persons. For coarse-grained movements, HAR-SAnet [21] proposes a UWB-based human activity recognition system. It adopts a convolutional neural network to automatically identify features instead of feeding the handcraft features of RF signals into a classifier. Seven commonly seen activities are classified with an accuracy of 97.4%. All these works place the UWB device on tables or walls and the UWB device is static.

8 LIMITATIONS AND DISCUSSIONS

Possible interference: When there are other moving subjects near the target, the reflections from other subjects can cause interference. The good news is that the large frequency bandwidth (1.5 GHz) of UWB signals brings fine resolution in resolving signals from different objects. As long as the interferer is not too close to the target, the two signals can still be separated without causing interference. Based on our experience, for human respiration sensing, if another walking person (interferer) is not within 20 cm of the target, accurate respiration sensing can still be achieved. However, if the interferer moves even closer, the performance degrades.

High speed mobility: In this work, Mobi^{2}Sense targets removing the device mobility caused by natural hand holding and robot movement. The device speed is not very fast. When we wave our hand dramatically at a very high speed (4-5 m/s), we do observe a performance degradation. We believe this is because high speed induces large Doppler shift which can cause phase measurement errors. Also the larger speed requires our system to adjust the compensation coefficient at a higher rate, causing larger errors.

Apply the proposed method on other wireless signals: The proposed method can be applied to other wireless signals such as FMCW radar and chirp-based acoustic signals. However, it can not be applied to narrow-band wireless technologies such as WiFi and LoRa, as the limited bandwidth cannot provide fine-enough spatial resolution for the proposed reference-based cancellation scheme to work. It is worth mentioning that the up-to-come 802.11be (WiFi 7) standard will adopt a large frequency bandwidth up to 320 MHz, and it is likely the proposed scheme can be applied on the next-generation WiFi.

Application scenarios: The first application scenario is to enable wireless sensing on robot when the robot is moving. For example, a robot is moving and the user would like to use a gesture which can be sensed by the RF module on the robot to change the robot's moving direction. Without the proposed method, the robot needs to stop to sense the gesture and the dilemma is that the robot needs to sense there is a gesture to stop. Another interesting application scenario we envision is to integrate wireless sensing with drone to enable applications which require high mobility such as sensing the soil moisture in a farm covering an area of tens of kilometers. The drone's movement and motor-induced vibration would severely interfere with wireless sensing. Compared with a robot, the drone can freely move in 3D and the movement pattern is more complicated. The complex device motions need to be tackled before wireless sensing can work on a drone.

9 CONCLUSION

Although contactless sensing has been studied for years, a missing piece which has not been studied is the effect of device motion on sensing. We theoretically model the impact of device motion on sensing and propose novel signal processing schemes to cancel the effect of device motion to enable sensing with mobility. We demonstrate the effectiveness of the proposed system using three real-life applications. We believe this is a new sensing modality which combines wireless sensing with mobility, moving a critical step towards true mobile and ubiquitous sensing.

ACKNOWLEDGMENTS

This work is partially supported by the National Natural Science Foundation of China (No. 62172394, No. 62072450), the Tencent Mobility Research Fund T160-CSIG-2022053100001, the Youth Innovation Promotion Association, Chinese Academy of Sciences (No. 2020109), the EU Horizon 2020 research and innovation programme IDEA-FAST (No. 853981), and the EU CHIST-ERA RadioSense Project.

REFERENCES

[1] 2002. *FCC Rules Regarding Ultra-Wideband.* Retrieved April 22, 2002 from https://transition.fcc.gov/Bureaus/Engineering_Technology/Orders/2002/fcc02048.pdf
[2] 2011. *WiFI card.* https://dhalperi.github.io/linux-80211n-csitool/index.html
[3] 2013. Whole-Home Gesture Recognition Using Wireless Signals. In *Proceedings of the 19th Annual International Conference on Mobile Computing and Networking (MobiCom '13).* Association for Computing Machinery, 27–38.
[4] 2017. x4-uwb-radar-soc. https://www.electronicspecifier.com/products/micros/sensors-benefit-from-latest-x4-uwb-radar-soc.
[5] 2019. Heal-Force PC3000. http://www.healforce.com/en/html/products/healthcareequipment/patientmonitor/608.html.
[6] 2020. MmVib: Micrometer-Level Vibration Measurement with Mmwave Radar. In *Proceedings of the 26th Annual International Conference on Mobile Computing and Networking (MobiCom '20).* Association for Computing Machinery, Article 45, 13 pages.
[7] 2020. Novelda AS X4. https://novelda.com/x4-soc.html.
[8] 2020. *Xiaomi Introduces Groundbreaking UWB Technology.* Retrieved October 13, 2020 from https://blog.mi.com/en/2020/10/13/xiaomi-introduces-groundbreaking-uwb-technology/

[9] 2021. Respiration Monitor Belt logger sensor NUL-236. https://neulog.com/respiration-monitor-belt/.

[10] 2021. Ultra Wideband availability. Retrieved April 20, 2021 from https://support.apple.com/en-us/HT212274

[11] 2021. VIVE Tracker. https://www.vive.com/.

[12] 2022. *Qualisys.* Retrieved June 28, 2022 from https://www.qualisys.com/

[13] Fadel Adib, Zachary Kabelac, and Dina Katabi. 2015. Multi-Person Localization via RF Body Reflections. In *Proceedings of the 12th USENIX Conference on Networked Systems Design and Implementation (NSDI'15)*. USENIX Association, 279–292.

[14] Fadel Adib, Zach Kabelac, Dina Katabi, and Robert C. Miller. 2014. 3D Tracking via Body Radio Reflections. In *11th USENIX Symposium on Networked Systems Design and Implementation (NSDI 14)*. USENIX Association, 317–329.

[15] Fadel Adib and Dina Katabi. 2013. See through Walls with WiFi!. In *Proceedings of the ACM SIGCOMM 2013 Conference on SIGCOMM (SIGCOMM '13)*. Association for Computing Machinery, New York, NY, USA, 75–86.

[16] Novelda AS. 2021. X4 - Datasheet. https://www.radartutorial.eu/19.kartei/13.labs/pubs/x4_datasheet_revE_restricted.pdf.

[17] Chao Cai, Henglin Pu, Liyuan Ye, Hongbo Jiang, and Jun Luo. 2021. Active Acoustic Sensing for Hearing Temperature under Acoustic Interference. *IEEE Transactions on Mobile Computing* (2021), 1–1.

[18] Zhaoxin Chang, Fusang Zhang, Jie Xiong, Junqi Ma, Beihong Jin, and Daqing Zhang. 2022. Sensor-free Soil Moisture Sensing Using LoRa Signals. *Proc. ACM Interact. Mob. Wearable Ubiquitous Technol.* 6, 2, Article 45 (June 2022), 27 pages.

[19] Weiyan Chen, Kai Niu, Deng Zhao, Rong Zheng, Dan Wu, Wei Wang, Leye Wang, and Daqing Zhang. 2020. Robust Dynamic Hand Gesture Interaction using LTE Terminals. In *2020 19th ACM/IEEE International Conference on Information Processing in Sensor Networks (IPSN)*. 109–120.

[20] Yu-Yao Chen, Shih-Ping Huang, Ting-Wei Wu, Wei-Ting Tsai, Chong-Yi Liou, and Shau-Gang Mao. 2020. UWB System for Indoor Positioning and Tracking With Arbitrary Target Orientation, Optimal Anchor Location, and Adaptive NLOS Mitigation. *IEEE Transactions on Vehicular Technology* 69, 9 (2020), 9304–9314.

[21] Zhe Chen, Chao Cai, Tianyue Zheng, Jun Luo, Jie Xiong, and Xin Wang. 2021. RF-Based Human Activity Recognition Using Signal Adapted Convolutional Neural Network. *IEEE Transactions on Mobile Computing* (2021), 1–1.

[22] Ziyang Chen, Panlong Yang, Jie Xiong, Yuanhao Feng, and Xiang-Yang Li. 2020. TagRay: Contactless Sensing and Tracking of Mobile Objects using COTS RFID Devices. In *IEEE INFOCOM 2020 - IEEE Conference on Computer Communications*. 307–316.

[23] Zhe Chen, Tianyue Zheng, Chao Cai, and Jun Luo. 2021. MoVi-Fi: Motion-Robust Vital Signs Waveform Recovery via Deep Interpreted RF Sensing. In *Proceedings of the 27th Annual International Conference on Mobile Computing and Networking (MobiCom '21)*. Association for Computing Machinery, New York, NY, USA, 392–405.

[24] Zhe Chen, Tianyue Zheng, and Jun Luo. 2021. Octopus: A Practical and Versatile Wideband MIMO Sensing Platform. In *Proceedings of the 27th Annual International Conference on Mobile Computing and Networking (MobiCom '21)*. Association for Computing Machinery, New York, NY, USA, 601–614.

[25] Nitin Dahad. 2020. Lenovo adds Novelda UWB sensor for human presence detection in ThinkPad. Retrieved November 5, 2020 from https://www.embedded.com/lenovo-adds-novelda-uwb-sensor-for-human-presence-detection-in-thinkpad/

[26] Shuya Ding, Zhe Chen, Tianyue Zheng, and Jun Luo. 2020. *RF-Net: A Unified Meta-Learning Framework for RF-Enabled One-Shot Human Activity Recognition*. Association for Computing Machinery, New York, NY, USA, 517–530.

[27] Walter Gander, Gene H. Golub, and Rolf Strebel. 1994. Least-squares fitting of circles and ellipses. *BIT Numerical Mathematics* 34, 4 (1994), 558–578.

[28] Ruiyang Gao, Wenwei Li, Yaxiong Xie, Enze Yi, Leye Wang, Dan Wu, and Daqing Zhang. 2022. Towards Robust Gesture Recognition by Characterizing the Sensing Quality of WiFi Signals. *Proc. ACM Interact. Mob. Wearable Ubiquitous Technol.* 6, 1, Article 11 (mar 2022), 26 pages. https://doi.org/10.1145/3517241

[29] Unsoo Ha, Salah Assana, and Fadel Adib. 2020. Contactless Seismocardiography via Deep Learning Radars. In *Proceedings of the 26th Annual International Conference on Mobile Computing and Networking (MobiCom '20)*. Association for Computing Machinery, Article 62, 14 pages.

[30] Unsoo Ha, Junshan Leng, Alaa Khaddaj, and Fadel Adib. 2020. Food and Liquid Sensing in Practical Environments using RFIDs. In *17th USENIX Symposium on Networked Systems Design and Implementation (NSDI 20)*. USENIX Association, Santa Clara, CA, 1083–1100.

[31] Wenjun Jiang, Chenglin Miao, Fenglong Ma, Shuochao Yao, Yaqing Wang, Ye Yuan, Hongfei Xue, Chen Song, Xin Ma, Dimitrios Koutsonikolas, Wenyao Xu, and Lu Su. 2018. Towards Environment Independent Device Free Human Activity Recognition *(MobiCom '18)*. Association for Computing Machinery, 289–304.

[32] Wenjun Jiang, Hongfei Xue, Chenglin Miao, Shiyang Wang, Sen Lin, Chong Tian, Srinivasan Murali, Haochen Hu, Zhi Sun, and Lu Su. 2020. Towards 3D Human Pose Construction Using Wifi. In *Proceedings of the 26th Annual International Conference on Mobile Computing and Networking (MobiCom '20)*. Association for Computing Machinery, Article 23, 14 pages.

[33] T L Lai, H Robbins, and C Z Wei. 1978. Strong consistency of least squares estimates in multiple regression. *Proceedings of the National Academy of Sciences of the United States of America* 75, 7 (07 1978), 3034–3036.

[34] Siheng Li, Zhi Wang, Fusang Zhang, and Beihong Jin. 2022. Fine-Grained Respiration Monitoring During Overnight Sleep Using IR-UWB Radar. In *Mobile and Ubiquitous Systems: Computing, Networking and Services*, Takahiro Hara and Hirozumi Yamaguchi (Eds.). Springer International Publishing, Cham, 84–101.

[35] Kang Ling, Yuntang Liu, Ke Sun, Wei Wang, Lei Xie, and Qing Gu. 2020. SpiderMon: Towards Using Cell Towers as Illuminating Sources for Keystroke Monitoring. In *IEEE INFOCOM 2020 - IEEE Conference on Computer Communications*. 666–675.

[36] Wenguang Mao, Jian He, and Lili Qiu. 2016. CAT: High-Precision Acoustic Motion Tracking. In *Proceedings of the 22nd Annual International Conference on Mobile Computing and Networking (MobiCom '16)*. Association for Computing Machinery, 69–81.

[37] Sharef Neemat, Oleg Krasnov, and Alexander Yarovoy. 2019. An Interference Mitigation Technique for FMCW Radar Using Beat-Frequencies Interpolation in the STFT Domain. *IEEE Transactions on Microwave Theory and Techniques* 67, 3 (2019), 1207–1220.

[38] Kai Niu, Fusang Zhang, Xuanzhi Wang, Qin Lv, Haitong Luo, and Daqing Zhang. 2021. Understanding WiFi Signal Frequency Features for Position-Independent Gesture Sensing. *IEEE Transactions on Mobile Computing* (2021), 1–1.

[39] Robin Raju, Greg E. Bridges, and Sharmistha Bhadra. 2020. Wireless Passive Sensors for Food Quality Monitoring: Improving the Safety of Food Products. *IEEE Antennas and Propagation Magazine* 62, 5 (2020), 76–89. https://doi.org/10.1109/MAP.2020.3003216

[40] Reeman Robot. 2021. Reeman robot. https://www.reeman.cn/products/robot/trooper.

[41] Deepak Singh. 2021. What is Ultra-Wideband (UWB) technology on Samsung Phones? How is it helpful? Retrieved May 4, 2021 from https://www.smartprix.com/bytes/phones-with-uwb-ultrawideband-connectivity/

[42] Xingzhe Song, Boyuan Yang, Ge Yang, Ruirong Chen, Erick Forno, Wei Chen, and Wei Gao. 2020. SpiroSonic: Monitoring Human Lung Function via Acoustic Sensing on Commodity Smartphones. In *Proceedings of the 26th Annual International Conference on Mobile Computing and Networking (MobiCom '20)*. Association for Computing Machinery, Article 52, 14 pages.

[43] Matthias Wagner, Fisnik Sulejmani, Alexander Melzer, Paul Meissner, and Mario Huemer. 2018. Threshold-Free Interference Cancellation Method for Automotive FMCW Radar Systems. In *2018 IEEE International Symposium on Circuits and Systems (ISCAS)*. 1–4.

[44] Anran Wang, Jacob E. Sunshine, and Shyamnath Gollakota. 2019. Contactless Infant Monitoring Using White Noise. In *The 25th Annual International Conference on Mobile Computing and Networking (MobiCom '19)*. Association for Computing Machinery, Article 52, 16 pages.

[45] Hao Wang, Daqing Zhang, Junyi Ma, Yasha Wang, Yuxiang Wang, Dan Wu, Tao Gu, and Bing Xie. 2016. Human Respiration Detection with Commodity Wifi Devices: Do User Location and Body Orientation Matter?. In *Proceedings of the 2016 ACM International Joint Conference on Pervasive and Ubiquitous Computing* (Heidelberg, Germany) *(UbiComp '16)*. Association for Computing Machinery, New York, NY, USA, 25–36.

[46] Ju Wang, Jie Xiong, Xiaojiang Chen, Hongbo Jiang, Rajesh Krishna Balan, and Dingyi Fang. 2017. TagScan: Simultaneous Target Imaging and Material Identification with Commodity RFID Devices. In *Proceedings of the 23rd Annual International Conference on Mobile Computing and Networking (MobiCom '17)*. Association for Computing Machinery, 288–300.

[47] Ju Wang, Jie Xiong, Hongbo Jiang, Kyle Jamieson, Xiaojiang Chen, Dingyi Fang, and Chen Wang. 2018. Low Human-Effort, Device-Free Localization with Fine-Grained Subcarrier Information. *IEEE Transactions on Mobile Computing* 17, 11 (2018), 2550–2563.

[48] Wei Wang, Alex X. Liu, Muhammad Shahzad, Kang Ling, and Sanglu Lu. 2015. Understanding and Modeling of WiFi Signal Based Human Activity Recognition. In *Proceedings of the 21st Annual International Conference on Mobile Computing and Networking (MobiCom '15)*. Association for Computing Machinery, 65–76.

[49] Wei Wang, Alex X Liu, Muhammad Shahzad, Kang Ling, and Sanglu Lu. 2015. Understanding and modeling of wifi signal based human activity recognition. In *Proceedings of the 21st annual international conference on mobile computing and networking*. 65–76.

[50] Zirui Wang, Shaoxian Li, Zhengyuan Zhang, Fan Lv, and Yanzhao Hou. 2018. Research on UWB Positioning Accuracy in Warehouse Environment. *Procedia Computer Science* 131 (2018), 946–951. Recent Advancement in Information and Communication Technology:.

[51] Zhi Wang, Fusang Zhang, Siheng Li, and Beihong Jin. 2021. Exploiting Passive Beamforming of Smart Speakers to Monitor Human Heartbeat in Real Time. In *2021 IEEE Global Communications Conference (GLOBECOM)*. 1–6.

[52] Teng Wei and Xinyu Zhang. 2015. MTrack: High-Precision Passive Tracking Using Millimeter Wave Radios. In *Proceedings of the 21st Annual International Conference on Mobile Computing and Networking (MobiCom '15)*. Association for Computing Machinery, 117–129.

[53] Dan Wu, Ruiyang Gao, Youwei Zeng, Jinyi Liu, Leye Wang, Tao Gu, and Daqing Zhang. 2020. FingerDraw: Sub-Wavelength Level Finger Motion Tracking with WiFi Signals. *Proc. ACM Interact. Mob. Wearable Ubiquitous Technol.* 4, 1, Article 31 (mar 2020), 27 pages.

[54] Dan Wu, Daqing Zhang, Chenren Xu, Hao Wang, and Xiang Li. 2017. Device-Free WiFi Human Sensing: From Pattern-Based to Model-Based Approaches. *IEEE Communications Magazine* 55, 10 (2017), 91–97.

[55] Binbin Xie, Jie Xiong, Xiaojiang Chen, Eugene Chai, Liyao Li, Zhanyong Tang, and Dingyi Fang. 2019. Tagtag: Material Sensing with Commodity RFID *(SenSys '19)*. Association for Computing Machinery, New York, NY, USA, 338–350.

[56] Binbin Xie, Jie Xiong, Xiaojiang Chen, and Dingyi Fang. 2020. Exploring Commodity RFID for Contactless Sub-Millimeter Vibration Sensing. In *Proceedings of the 18th Conference on Embedded Networked Sensor Systems (SenSys '20)*. Association for Computing Machinery, 15–27.

[57] Panlong Yang, Yuanhao Feng, Jie Xiong, Ziyang Chen, and Xiang-Yang Li. 2020. RF-Ear: Contactless Multi-device Vibration Sensing and Identification Using COTS RFID. In *IEEE INFOCOM 2020 - IEEE Conference on Computer Communications*. 297–306.

[58] Yanni Yang, Jiannong Cao, Xiulong Liu, and Xuefeng Liu. 2019. Multi-Breath: Separate Respiration Monitoring for Multiple Persons with UWB Radar. In *2019 IEEE 43rd Annual Computer Software and Applications Conference (COMPSAC)*, Vol. 1. 840–849.

[59] Youwei Zeng, Dan Wu, Jie Xiong, Enze Yi, Ruiyang Gao, and Daqing Zhang. 2019. FarSense: Pushing the Range Limit of WiFi-Based Respiration Sensing with CSI Ratio of Two Antennas. *Proc. ACM Interact. Mob. Wearable Ubiquitous Technol.* 3, 3, Article 121 (Sept. 2019), 26 pages.

[60] Daqing Zhang, Hao Wang, and Dan Wu. 2017. Toward Centimeter-Scale Human Activity Sensing with Wi-Fi Signals. *Computer* 50, 1 (2017), 48–57. https://doi.org/10.1109/MC.2017.7

[61] Daqing Zhang, Youwei Zeng, Fusang Zhang, and Jie Xiong. 2022. Chapter 11 - WiFi CSI-based vital signs monitoring. In *Contactless Vital Signs Monitoring*, Wenjin Wang and Xuyu Wang (Eds.). Academic Press, 231–255.

[62] Daqing Zhang, Fusang Zhang, Dan Wu, Jie Xiong, and Kai Niu. 2021. *Fresnel Zone Based Theories for Contactless Sensing*. Springer International Publishing, Cham, 145–164.

[63] Fusang Zhang, Zhaoxin Chang, Kai Niu, Jie Xiong, Beihong Jin, Qin Lv, and Daqing Zhang. 2020. Exploring LoRa for Long-Range Through-Wall Sensing. *Proc. ACM Interact. Mob. Wearable Ubiquitous Technol.* 4, 2, Article 68 (June 2020), 27 pages.

[64] Fusang Zhang, Zhaoxin Chang, Jie Xiong, Rong Zheng, Junqi Ma, Kai Niu, Beihong Jin, and Daqing Zhang. 2021. Unlocking the Beamforming Potential of LoRa for Long-Range Multi-Target Respiration Sensing. *Proc. ACM Interact. Mob. Wearable Ubiquitous Technol.* 5, 2, Article 85 (June 2021), 25 pages.

[65] Fusang Zhang, Kai Niu, Xiaolai Fu, and Beihong Jin. 2020. AcousticThermo: Temperature Monitoring Using Acoustic Pulse Signal. In *2020 16th International Conference on Mobility, Sensing and Networking (MSN)*. 683–687.

[66] Fusang Zhang, Kai Niu, Jie Xiong, Beihong Jin, Tao Gu, Yuhang Jiang, and Daqing Zhang. 2019. Towards a Diffraction-Based Sensing Approach on Human Activity Recognition. *Proc. ACM Interact. Mob. Wearable Ubiquitous Technol.* 3, 1, Article 33 (March 2019), 25 pages.

[67] Fusang Zhang, Zhi Wang, Beihong Jin, Jie Xiong, and Daqing Zhang. 2020. Your Smart Speaker Can "Hear" Your Heartbeat! *Proc. ACM Interact. Mob. Wearable Ubiquitous Technol.* 4, 4, Article 161 (dec 2020), 24 pages.

[68] Fusang Zhang, Daqing Zhang, Jie Xiong, Hao Wang, Kai Niu, Beihong Jin, and Yuxiang Wang. 2018. From Fresnel Diffraction Model to Fine-Grained Human Respiration Sensing with Commodity Wi-Fi Devices. *Proc. ACM Interact. Mob. Wearable Ubiquitous Technol.* 2, 1, Article 53 (March 2018), 23 pages.

[69] Mingmin Zhao, Fadel Adib, and Dina Katabi. 2016. Emotion Recognition Using Wireless Signals. (2016), 95–108.

[70] Mingmin Zhao, Yonglong Tian, Hang Zhao, Mohammad Abu Alsheikh, Tianhong Li, Rumen Hristov, Zachary Kabelac, Dina Katabi, and Antonio Torralba. 2018. RF-based 3D skeletons. In *Proceedings of the 2018 Conference of the ACM Special Interest Group on Data Communication*. 267–281.

[71] Tianyue Zheng, Zhe Chen, Chao Cai, Jun Luo, and Xu Zhang. 2020. V2iFi: In-Vehicle Vital Sign Monitoring via Compact RF Sensing. *Proc. ACM Interact. Mob. Wearable Ubiquitous Technol.* 4, 2, Article 70 (June 2020), 27 pages.

[72] Tianyue Zheng, Zhe Chen, Jun Luo, Lin Ke, Chaoyang Zhao, and Yaowen Yang. 2021. SiWa: see into walls via deep UWB radar. In *Proceedings of the 27th Annual International Conference on Mobile Computing and Networking*. 323–336.

[73] Tianyue Zheng, Zhe Chen, Shujie Zhang, Chao Cai, and Jun Luo. 2021. MoRe-Fi: Motion-Robust and Fine-Grained Respiration Monitoring via Deep-Learning UWB Radar. In *Proceedings of the 19th ACM Conference on Embedded Networked Sensor Systems (SenSys '21)*. Association for Computing Machinery, New York, NY, USA, 111–124.

[74] Xuezhao Zheng, Baoyuan Wang, and Ju Zhao. 2019. High-precision positioning of mine personnel based on wireless pulse technology. *PLOS ONE* 14, 7 (07 2019), 1–25.